Kinematic Design Method for a Rail Mounted Inspection Robot Arm

J.A.J. Huttenhuis

Faculty of Engineering Technology
Laboratory of Mechanical Automation
and Mechatronics

EXAMINATION COMMITTEE
dr.ir. R.K.G.M. Aarts
dr.ir. D.M. Brouwer
ir. D.J. Borgerink
prof.dr.ir. S. Stramigioli

WA

UNIVERSITY OF TWENTE.

Kinematic Design Method for a Rail Mounted Inspection Robot Arm

Master Thesis

of

Jop Anton Johan Huttenhuis

Born on 31, July 1982, in Enschede, The Netherlands.

Preface and acknowledgements

This master thesis marks the end of a study mechanical engineering at the University of Twente. During the education the curriculum fulfiled a broad interest in many different technical area's. But during a mechatronics project the true passion emerged. The combination of mechanical-, electrical-, control- and computer-engineering gives the field of mechatronics a pleasing diversity. And realizing that one has gained the knowledge to build devices based on these fields and actually make them work is a very rewarding experience. From all of the attended courses, one needs special attention, because without the knowledge gained during the course "Modern Robotics" the modeling and simulating would not have been so compact and elegantly. It is advised to all the interested readers to dive into this concept and learn to master it, because it will eventually become a very useful tool when dealing with the kinematics and dynamics of bodies.

Jop Huttenhuis

"Mechanical engineering is the application of science to the common purpose of life."

Author Unknown

Contents

THIS PAGE INTENTIONALLY LEFT BLANK

1 Introduction

This thesis is the result of a master assignment carried out at the University of Twente. The assignment originates from an interregional project named 'Roboship' as a part of the INTERREG IVA project 'SmartBot'.

A team consisting of 7 partners, DFKI Bremen, Imotec, Incas3, Meyer Werft, Univeristy of Groningen, Xsens and the University of Twente, worked on an independent and intelligent platform for inspection of ballast water tanks. When I was involved in the project, around november 2013, the project was already in an advanced stage. One of the issues that needed to be solved was designing and building a robotic arm.

After a few weeks of in depth reading, learning the mathematics of screw theory and meeting the other partners of the project, the work-flow marked the borders of what one could call a design-method. This method is the main part of this report and is written in the form of an academical paper. Although no brand new science is developed, the systematic structuring of the problem already showed great interest among other engineers even while the study was unfinished.

As it seems irrelevant for the method to show some specific details of the simulation, these are given in appendix A. The algorithm to obtain the elastic wrench is taken from [1] and listed in appendix B for quick reference purposes. Appendix C is dedicated to some aspects with respect to the design of the proof-of-principle, like considerations about the used actuators, choices for the bearing, a custom designed gear, a sleeve bearing and the deviation from the design rules.

Kinematic Design Method for a Rail Mounted Inspection Robot Arm

J.A.J. Huttenhuis[*,a], D.J. Borgerink[b,c], D.M. Brouwer[a], R.G.K.M. Aarts[a] and S. Stramigioli[b]

March 17, 2015

Abstract

A robotic-arm supported by a rail mounted platform is designed. The scenario of a Ballast Water Tank fitted with a rail is converted into a required workspace. Kinematic structures are synthesized and subjected to design criteria. A generic numerical inverse-kinematics method is described which uses the transposed Jacobian and an elastic wrench based on the framework of screw theory. A simulation is used to benchmark the kinematic structures. A proof-of-principle is build and used to validate the simulation results. *Keywords: redundant, inverse kinematics, multibody, confined space, ballast water tank, screw theory, elastic wrench*

1 Introduction

Ballast water tanks (BWT) are used in ships to maintain balance. They are filled and drained based on to the amount of cargo. As the BWTs are subject to serious fouling they need to be inspected regularly. Until today this is done manually through visual inspection and handheld measurement devices, e.g. ultrasonic thickness sensors. These inspections are labor intensive and costly because they can only take place when the ship is in a dry-dock [1]. Due to the complex structure of the tanks and additional obstacles such as pipes, stairs and manhols, it is difficult to automate the maintenance of BWTs. Potentially suitable robotic concepts for automated maintenance of BWTs include robofish [2], flying robots [3], magnetic crawlers [4] [5], legged robots [6] and cable-guided robots [7]. However, all these concepts have drawbacks in view of the structure of the tanks, limited payload or vulnerability to contamination inside the tanks. Currently there is no robotic-arm available which is foldable, has the required workspace and the appropriate weight versus stiffness for the BWT scenario.

In previous studies, Christensen et al. [8] showed that a rail-guided robotic system has the greatest potential. This robot requires a manipulator to position a sensor on the interior walls.

1.1 Problem

Borgerink[9] has shown that it is not desirable to have a single serial manipulator clamped on a compliant rail. A solution was found in a two stage concept, see fig. 1, where two serial manipulators are stacked, such that the large stroke arm positions an intermediate end-effector close to the point to be measured. This intermediate end-effector latches to the tank wall by means of an electromagnet. The small stroke arm positions the final end-effector, the sensor, on the point of interest.
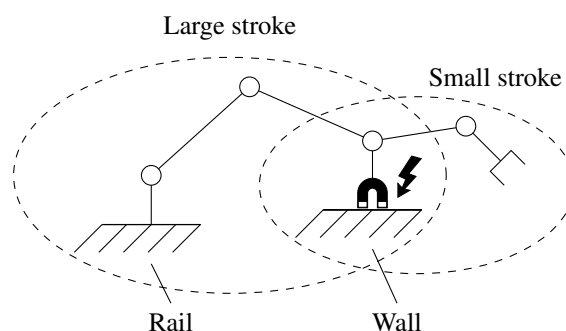
Figure 1: Two-stage arm concept, with a magnet as intermediate end-effector, latching to a wall.

The sensor has to be able to measure all interior points of the tank-wall. The sensor must be placed perpendicular to the wall, within 5° and with a position accuracy of 10mm. It is assumed that the small stroke manipulator has a workspace with a radius of 100mm. The envelope of the robotic-arm must be such that, when in stowed configuration, it does not collide with the walls when passing through the manholes inside a BWT. Furthermore, some redundancy is required to e.g. avoid obstacles or go around a corner.

So the question is: "What should the kinematic structure look like to satisfy the above requirements?"

As the inverse kinematics is a highly non-linear problem, in general, there exists no 'closed form' solution [10]. Therefore, a numerical solution for the inverse kinematics needs to be found.

1.2 Goal

The primary purpose of this paper is to describe the generic method to generate kinematic models and to evaluate their

---

[*]Corresponding author: jophuttenhuis@gmail.com
[a]Mechanical Automation & Mechatronics, University of Twente.
[b]Robotics and Mechatronics, University of Twente.
[c]INCAS[3], Assen, The Netherlands.

suitability for a certain scenario. This paper will focus only on the large-stroke stage and therefore the intermediate end-effector, the magnet. The steps required to come up with a kinematic design given the boundary conditions will be described. The secondary purpose is to show the implementation by means of a realized proof-of-concept build for demonstration purposes.

1.3 Outline

In section 2 the method is presented. The steps required to end up with a simulation of a kinematic structure are explained. First is explained how a scenario can be converted into a set of relative poses. Then the notation for kinematic models is explained. The inverse kinematics are explained by means of an iterative algorithm. Finally the steps are combined to be able to run simulations. In section 3 the method is applied to the BWT scenario. One of the obtained kinematic structures is used to implement a proof-of-principle. This robotic arm is presented in section 4.

2 Method

In this section the general approach to find a kinematic structure will be explained. Geometrical and structural requirements like link dimensions or stiffness will not be taken into account. Instead of designing a kinematic structure and evaluating the resulting workspace in this method relative poses and candidate models are taken as starting point and are evaluated by simulation.

The position and orientation of a certain frame, e.g. the end-effector, with respect to another frame, e.g. the base, is called a pose. When no reference frame is mentioned the global inertial frame is used.

The purpose of the simulation is to evaluate whether a candidate-model is able to reach all required poses. To answer this question the following is required:

1. Desired poses for the end-effector must be given

2. A kinematic model must be known

3. A method that yields the joint-coordinates

These requirements are explained in the following subsections.

2.1 Scenario simplification

Usually the workspace of a robotic arm is expressed w.r.t. a fixed base. For a rail mounted system the reachable workspace is more complicated as the base is able to move along a rail track. It is useful to simplify this scenario. A scenario consists of a set of desired end-effector poses and a rail-system on which the base of the robot can position itself. Certain aspects of the scenario can be exploited to obtain a model that is simple yet sufficient. For example the rail can be installed such that it is parallel to large sections of the walls. It is then possible to define a limited set

of target-poses for the end-effector which need to be evaluated for reachability.

Figure 2 is used to illustrate the simplification process in case the rail is positioned parallel with a straight wall. The rail is assumed to be a straight path between Ψ_A and $\Psi_{A'}$. A flat wall, at a certain distance and parallel to the rail, is indicated by the yellow rectangle. Close to each corner of the wall a frame is defined, these denote the desired end-effector poses and are a function of the system requirements. Now the pose of Ψ_1 and Ψ_2 can be expressed in frame Ψ_A. As the base of the robot is able to move along the rail between Ψ_A and $\Psi_{A'}$, every point between Ψ_1 and $\Psi_{1'}$ would yield an identical relative pose. Furthermore, as the frames Ψ_1 and Ψ_2 are extremes in the sense of maximum distance from Ψ_A, it is assumed that when Ψ_1 and Ψ_2 are reachable every point between them is also reachable.

In fig. 3 a corner section is modeled with a top, bottom and two back walls. A quarter bend rail is installed and starts in the center of the front-left plane (not shown) and ends in the center of the front-right plane (not shown). Although the robot is able to move continuous along the curved rail, only three base poses are chosen at the beginning, half way and end of the bend. These are denoted as Ψ_A, Ψ_B and Ψ_C. For the front-right corner the frames Ψ_1 and Ψ_2 denote the desired end-effector pose with the normal direction facing outward. They should be reachable
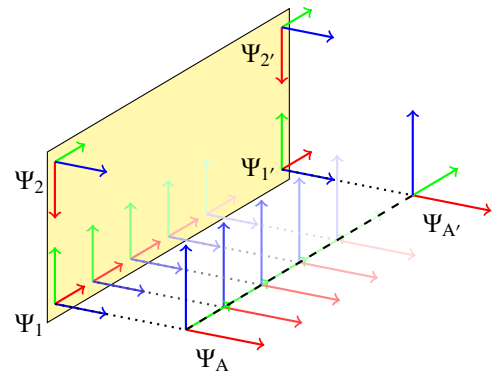
Figure 2: Base- and end-effector poses along a straight wall
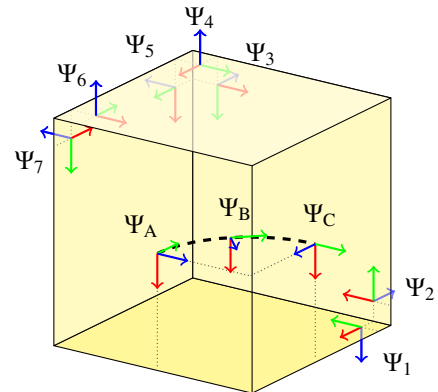
Figure 3: Three base- and seven end-effector poses in a corner section with a bent rail. For clarity the front-left and -right plane are not shown.

from pose Ψ_C. For the top-back corner the frame Ψ_3, Ψ_4 and Ψ_5 are selected, and should be reachable from pose Ψ_B. For the top-left corner the frames Ψ_6 and Ψ_7 are selected and should be reachable from pose Ψ_A. Although the other corners are also included in the model during simulation, for the purpose of clarity they are omitted in this figure.

It is essential to realize that only the relative position and orientation from the base of the manipulator to the required end-pose are relevant. Therefore, by identifying the required end-effector positions and choosing base positions, a finite set of relative poses is obtained that should be reachable. They are conveniently expressed as homogeneous transformation matrices, and are used in section 2.3 to calculate the inverse kinematics and in section 2.4 for simulation purposes.

2.2 Model synthesis

A kinematic structure is a set of links interconnected by joints. This method focuses on serial mechanisms with rigid links. The links and joints can be captured in a generic structure using screw theory [11]. The individual links can be described as constant transformation matrices whereas the joints are described by finite twists. The dynamics of the systems are discarded at this point, as only the kinematics are considered. Self-intersection of links and joint limits is ignored, as this depends on the geometry of the links.

As an example the kinematic structure of a 2-DOF manipulator with rotational joints in its initial configuration, shown in fig. 4, will be described. The inertial frame is denoted by Ψ_0. The pose of joint 1 is denoted by Ψ_1 and is described as a constant homogeneous transformation matrix H_1^0, thus Ψ_1 is fixed w.r.t. the base. Frame $\Psi_{1'}$ is attached to link 1 and is obtained after applying the joint transformation. The motion of joint 1 is described as a unit twist T_1 and is expressed in frame Ψ_1 the amount of motion is denoted by θ_1. Frame Ψ_2 denotes the pose of joint 2 and is expressed as H_2^1. Analogue to joint 1, T_2 describes the motion of joint 2 and determines the pose of frame $\Psi_{2'}$. It is now possible to describe the transformation H_e^0 from the end-effector coordinate frame to the base frame using
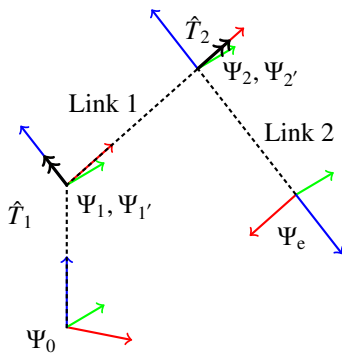
Figure 4: Example of a 2-DOF kinematic structure

screw theory notation:

$$H_e^0 = H_1^0 e^{\tilde{T}_{1'}^1} H_2^{1'} e^{\tilde{T}_{2'}^2} H_e^{2'} \qquad (1)$$

Where H_a^b are homogeneous transformation matrices used to map coordinates from frame a to frame b, and $e^{\tilde{T}_a^b}$ is the exponential format of the finite twist $\tilde{T}$.

The link lengths and joint orientations are captured in the H-matrices. Using this notation any serial chain can be described.

2.3 Inverse Kinematics

2.3.1 Introduction

Inverse-kinematics (IK) is referred to as the problem of finding the joint-coordinates given the end-effector pose. It involves solving a nonlinear set of equations, and although for some specific kinematic structures a closed-form solution is available, in general it is not. In the case the robotic arm has more DOFs than the end-effector has constraints, the structure is redundant and in general there are infinite IK solutions. Furthermore, when the desired end-effector pose is outside the reachable area there exists no solution.

Multiple techniques are available for solving the IK problem such as transposed Jacobian, pseudoinverse and damped least squares method [12]. The transposed Jacobian method is used as it can be implemented using an elastic wrench in a straightforward manner. Furthermore, it is fast and relatively easy to compute.

2.3.2 Transposed Jacobian method

The geometrical Jacobian J, is used in forward kinematics as a map from joint velocities $\dot{\theta}$, to end-effector twist T.

$$T = J(\theta)\dot{\theta} \qquad (2)$$

Due to duality the transposed Jacobian is the map from a wrench W, acting on the end-effector, to joint-torques τ.

$$\tau^\top = J^\top(\theta)w^\top \qquad (3)$$

When a translational and a rotational spring are modeled between the end-effector frame and the desired frame, these springs will naturally pull the end-effector into place. The stiffness of the springs determine the convergence rate. The springs can be combined and generalized to a wrench. This elastic wrench is the key component of the algorithm and was presented by Stramigioli [13]. With the wrench modeled as an elastic element between the end-effector and the desired location, its magnitude can be seen as a measure of error. An iterative algorithm is implemented which goal is to minimize this error by updating joint-coordinates.

2.3.3 Elastic Wrench

Where a conventional spring can be seen as a one dimensional element, the elastic wrench is a spatial element. Using [13] and [14] it is defined as a generalized force and

torque caused by misalignment of two different frames. By attaching one frame to the end-effector and the other to the desired pose, the misalignment can be expressed as H_e^d. Using this displacement and a stiffness K, an elastic element can be modeled:

$$w_e = w_e(K, H_e^d) \qquad (4)$$

The reaction torques for static equilibrium can be calculated using Equation eq. (3). The sign and magnitude of the torques indicate how to move the joints to minimize the wrench.

For large values of the wrench the joint update become large, this can lead to unstable simulation results. Therefore the magnitude of the joint update is limited.

2.3.4 Iterative Algorithm

The robotic-arm starts in an initial configuration, e.g. straight up. An elastic wrench is calculated using eq. (4) and applied to the end-effector which depends on the pose of the end-effector with respect to the required end-pose and a certain stiffness. In this configuration, the joint torques can be calculated for static equilibrium using eq. (3). Then all joints coordinates can be updated using the induced reaction torques. Hereby the end-effector will move toward the required end-pose and the magnitude of the elastic wrench will decrease. This process is repeated until the end-effector pose is within a certain range.

The algorithm uses only the kinematic structure to find a feasible solution. There are no dynamics involved as no assumptions with respect to mass or inertia are being made. It does not check for collision with itself or maximum joint limits, these aspects are related to the geometric design. In general, the solution is dependent on the initial configuration and the choice of the spatial stiffness K.

The algorithm suffers from local minima when the links are *asymmetric*. One way to avoid this is to make the links symmetric, as illustrated in fig. 6. A link is called symmetric if the axes of the two connected joints are co-planar.

2.4 Simulation

The purpose of the simulation is to evaluate every kinematic model for all obtained relative poses using the IK-algorithm. When a joint configuration has been found where the end-effector is within a certain range w.r.t. position and orientation, the combination of model and pose is marked as 'success'. The joint configuration is stored and the next pose is evaluated. The process is illustrated by the flowchart in fig. 5.

The required pose might be outside the reachable workspace of the end-effector, the model will move as close as possible to the required pose. To prevent an infinite loop the process is aborted when the number of iterations exceeds a certain limit. The combination of model and pose is marked as 'failed'.

3 Implementation

To give the general approach more meaning it is applied to a real world application. The use case consists of designing the kinematic structure of a manipulator on a rail guided robotic platform in a BWT.

3.1 Scenario simplification

The scenario is given by an experimental tank, whose dimensions are actual sizes. A modular rail system is installed inside the tank. As the tank consists of many flat surfaces it is assumed that if the end-effector can reach all corners, it can reach the whole surface.

The process of mapping coordinates of the experimental tank to relative locations is explained on the basis of
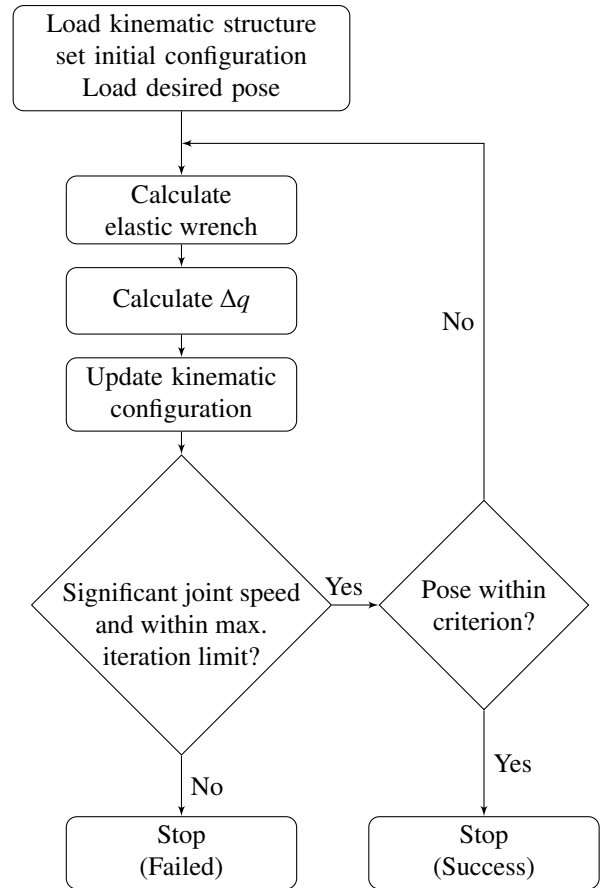
Figure 5: Inverse Kinematics Algorithm.
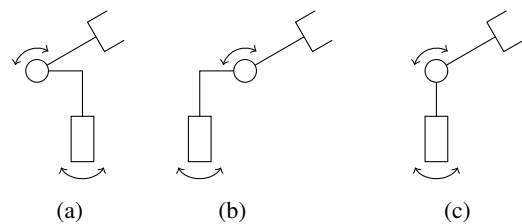
Figure 6: An asymmetric link shown in two different configurations in figs. 6a and 6b and a symmetric link in fig. 6c.

(a) Experimental tank   (b) Required workspace
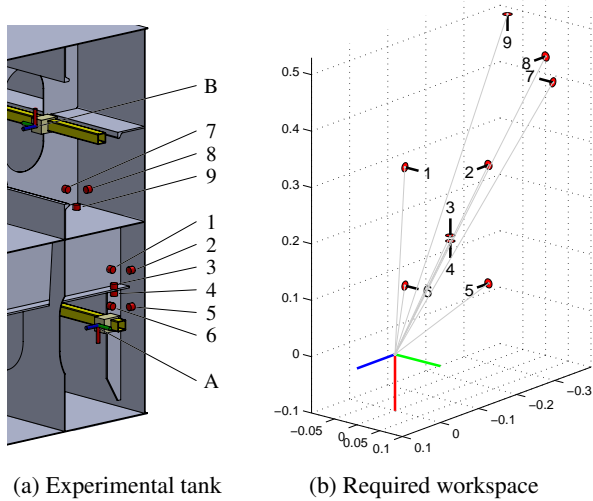
Figure 7: Mapping of tank locations to relative locations. The relative locations from the tank (fig. 7a) determine the required workspace (fig. 7b). For clarity only the normal direction of the required pose is shown.

an example. Figure 7 shows a section view of the experimental tank with two arbitrary starting positions on the rail in different compartments. The end-effector must be able to reach tank-locations 1 through 6 while at root-location A, and tank-locations 7 through 9 while at B. When all tank locations are expressed in the frame of their respective root-location, see fig. 7a, the required relative poses are obtained. Note the orientation of root-location B differs from A.

The coordinates of the corners are obtained from the CAD-drawings of the tank. The required pose of the intermediate end-effector is obtained using the coordinates of the corner, the direction of the surface normal and an offset distance of the corner. The second stage is considered to have a workspace with a radius of 100mm, this distance will be used as the offset. For the base of the manipulator a suitable pose can be obtained from the CAD-model. As the robot has a pre-defined orientation on the rail and because its locomotion has only one DOF, the shortest distance from the rail to the required end-effector pose is a plausible choice.

From the experimental tank a set of 303 relative poses are obtained. Many of the poses are similar due to the repetitive geometry of the BWT, when they are within 4mm and 1° from each other they are removed from the set. The remaining set of 169 relative poses will be used as the minimal performance criterion for the kinematic structure.

3.2 Model synthesis

As presented in section 2.2 the kinematic structure consists alternating link and joint elements. For simplicity reasons the joints types will be restricted to rotational. Furthermore, the orientation of the axis of motion will be limited to roll-, pitch- and yaw-joints base on the longitudinal di-

rection of the prior link as illustrated in fig. 8 .

By exploiting some of the properties of the system, certain design rules can be deduced. The intermediate end-effector consists of a magnet that needs to be positioned perpendicular to the walls. Since the small stroke arm will be able to rotate around the longitudinal axis of the end-effector, the orientation about this axis is irrelevant. Therefore, a 5 DOF robotic arm is the minimal requirement. But as BWT's have obstacles like pipes and the rail itself some kind of kinematic redundancy is essential. Therefore, a 6 DOF robotic arm will be designed and evaluated.

One way to generate models is to create a model for every possible combination of joint types. In general for a n-DOF system with three types of joints this would yield 3^n possibilities. For the assumed 6 DOF system this yields 729 possible combinations. Fortunately, many of these have are irrelevant value. The following design rules will eliminate many models (joint numbering starts at the base):

(1) The longitudinal orientation of the end-effector is irrelevant therefore the last joint should not be a roll-joint.
(2) For the first joint a pitch- and yaw-joint are unfavor-

Pitch

Yaw

Roll

(a)   (b)
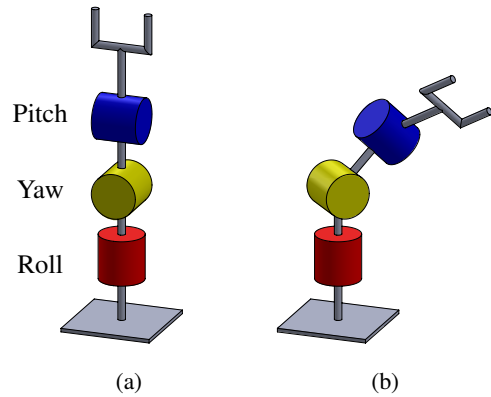
Figure 8: Roll- Yaw- and Pitch-joints in their initial (fig. 8a) and deformed (fig. 8b) configuration.

1   2   3   4   5
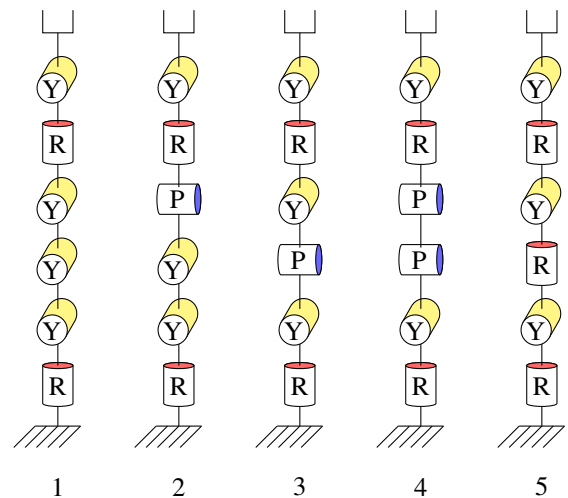
Figure 9: Candidate kinematic structures with (R)oll/(Y)aw/(P)itch-joint elements.

able. Their range is limited to prevent collision with the base.

(3) Two subsequent roll-joints introduce an internal mode with no advantages.

(4) After a roll-joint a pitch- and yaw-joint are effectively equal.

(5) To allow maximum orientational dexterity for the end-effector while maintaining maximum reachability, even when avoiding obstacles, the before last joint must be a roll-joint.

After applying these 'elimination rules' only five models are left, these are shown in fig. 9. Notice that these models only show the joint types and their order.

A complete kinematic model also needs link lengths, for which the following design rules were used. From the required workspace a maximum distance of 0.774m is obtained between base and desired pose. This yields the absolute minimal length. Foldability is required to shape the robotic-arm into a small envelope. This is necessary for maneuvering through manholes and making bends with a radius of 400mm. Folding can only be accomplished by yaw- and pitch- joints. As the maximum height to pass through manholes is 180mm this means for the candidates that the distance from the base to the first non-roll joint must be small. The same reasoning holds for the last link length. In this research no optimization is done with respect to the link length, they are chosen manually.

The longitudinal position of a roll-joint essentially does not change the kinematic structure, as long as it fits between the preceding and consecutive joint. Therefore a roll-joint effectively merges two individual link lengths into one effective length. Therefore the number of relevant link-length parameters to be chosen are equal to the number of non-roll joints plus one. For example, structure 5 in fig. 9 has 4 effective link lengths.

As stated above, the last end-effector link should be as short as possible for maximum reachability while still able to orientate. But to leave space to attach the second stange arm, a link length of 100mm was chosen. Furthermore for a compact envelope the first link length should also be minimal. After a design study the first effective link length turned out to be of a minimal length of approximately 50mm, the dimension is limited by the available sizes of the bearing and motors.

3.3 Inverse Kinematics

This section describes how the implementation of the method is done. For calculation of the elastic wrench the pose of the end-effector frame is expressed in the desired frame, this is calculated using eq. (5).

$$H_e^d = \left(H_d^0\right)^{-1} H_e^0 \tag{5}$$

The stiffness of the elastic wrench is set using the stiffness matrix K as denoted in eq. (6)

$$K = \begin{pmatrix} K_t & K_c \\ K_c{}^{\mathrm{T}} & K_o \end{pmatrix} \tag{6}$$

Where

$$K_t = \begin{pmatrix} 1 & 0 & 0 \\ 0 & 1 & 0 \\ 0 & 0 & 1 \end{pmatrix} \tag{7a}$$

$$K_o = \begin{pmatrix} 0.05 & 0 & 0 \\ 0 & 0.05 & 0 \\ 0 & 0 & 0 \end{pmatrix} \tag{7b}$$

$$K_c = \begin{pmatrix} 0 & 0 & 0 \\ 0 & 0 & 0 \\ 0 & 0 & 0 \end{pmatrix} \tag{7c}$$

Notice the translation-stiffness K_t has been set to unity. The orientational stiffness K_o has been set to 0.05 except for the direction along the z-axis. It is important the end-effector frame is oriented such that the local z-axis is aligned with the longitudinal direction of the sensor. The coupling stiffness K_c has been set equal to zero.

The maximum number of iterations is set to 10^4 steps. The values Δq are limited at $2°$. The end-effector position criterion is implemented as:

$$\left\| p_e^d \right\|^2 \leq d_{cr} \tag{8}$$

where p_e^d denotes the translation vector taken from the homogeneous matrix, and d_{cr} denotes the desired value of 5mm.

For the orientation criterion only the perpendicularity to the wall is important. This is implemented by calculating the angle between the z-axis of the end-effector with respect to the desired frame using the dot-product as:

$$\left(R_e^d \begin{pmatrix} 0 \\ 0 \\ 1 \end{pmatrix} \right) \bullet \begin{pmatrix} 0 \\ 0 \\ 1 \end{pmatrix} \leq \cos\left(\alpha_{cr}\right) \tag{9}$$

where R_e^d the rotation matrix taken from the homogeneous matrix, and α_{cr} denotes the orientation criterion of $5°$. In this case the left hand side reduces to the single element $H_e^d(3,3)$.

4 Results

4.1 Simulation results

In general the simulation of the generated models show they are all feasible structures. But when gradually reducing the total link length up to 1.076m, models 1, 2 and 4 showed many failures. Model 3 and 5 showed successful simulations down to a length of 0.808m, which results in an efficiency of 92% with respect to the Euclidean distance between the base and the required position. The only difference between these models is the type of the third joint, in model 3 this is a pitch- and in model 5 this is a roll-joint.

4.2 Proof of Principle

The robot-arm is mounted on a passive carrier pulled by the drive system, see fig. 11. The white plastic covers are added
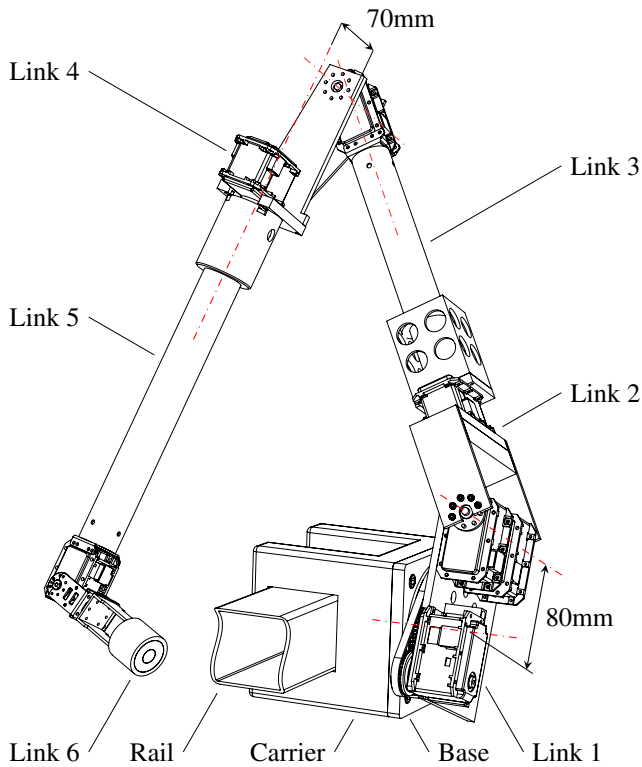
Figure 10: CAD model based on kinematic model 5. The asymmetric link 1 has an offset of 80mm, and link 4 has an offset of 70mm.

Figure 11: Proof of principle robot-arm, with covers, mounted on the drive unit. The relative pose of base- and end-effector is similar to the relative pose of Ψ_B and Ψ_3 from fig. 3.

for protecting electronic components and for aesthetic reasons. From a remote system, running Matlab, the setpoints for the Dynamixels are send by a wireless link. This way a pre-programmed path can be executed or the end-effector can be controlled by visual servoing.

The simulation showed model 5 as one of the feasible candidates. This model also inhibits the most recognizable null-space motion. Based on this kinematic model the CAD-model shown in fig. 10 is designed with Dynamixels MX-106 as actuators. The Dynamixels are not capable to withstand the bending torque induced on the roll joints. For the first (roll-)joint, a THK RA7008C-UU-C0 crossed-roller bearing yields the required support stiffness, and has small sizes. A 6mm GT2 timing belt and corresponding gears result in a 36:110 gear ratio for the first joint. The roll-joints 3 and 5 consist of coaxial tubes. The outer tube is fixed to the Dynamixel-housing, the inner tube is connected to the output shaft, and supported by a nylon bushing.

The symmetric-link design restriction was released for the first link, as collision of the second link with the rail was a major joint limitation. Furthermore, for joint 4, the succeeding link was offset in the direction of axis of rotation, this modification eliminates collision during folding. The (intermediate) end-effector consists of an electromagnet and forms the basis on which the second stage will be mounted.

5   Conclusion

The presented method is generic and can be used for many other scenarios. A complete description of a general approach to design serial kinematic mechanisms has been given. It is shown that for rail-mounted systems the core of the required workspace lies in the relative poses. A simple procedure is used to generate every possible candidate kinematic model using predefined joint types. Using elimination rules this set of candidate models is drastically reduced. Model generation is fast and structured but the rules dependent on the requirements.

A kinematic model does not imply the geometry of the links, therefore, at this stage it makes no sense to impose joint limits or implement collision detection. These aspects are of course essential for a mechanical design.

The inverse kinematics are obtained using a intuitive and natural approach. The algorithm is robust and does not suffer from instability due to singularities. When asymmetric links are modeled local minima can occur. The rate of convergence depends on the size of the update steps and the specified stiffness for the elastic wrench.

A proof-of-concept has been build, where the restriction for symmetry has been released for the first link. The choice for the modular actuators contributed to the ability to quickly (re-)build a mechanism. Although they did not meet their specifications they proof to be useful for the proof-of-principle.

References

[1] L. Christensen, J. Lemburg, T. Vögele, F. Kirchner, N. Fischer, R. Ahlers, G. Psarros, and L.-E. Etzold, "Tank inspection by cost effective rail based robots," in *Proceedings of the 15th International Conference*

on Computer Applications in Shipbuilding. International Conference on Computer Applications in Shipbuilding (ICCAS-11), 15th, September 20-22, Trieste, Italy, o.A., 9 2011.

[2] J. Liang, T. Wang, S. Wang, D. Zou, and J. Sun, "Experiment of robofish aided underwater archaeology," in *Proceedings of International Conference on Robotics and Biomimetics (ROBIO)*, 2005.

[3] A. Keemink, "Design, realization and analysis of a manipulation system for UAVs," Master's thesis, University of Twente, 2012.

[4] Focusproject: Ship Inspection Robot, ETH Zürich, http://www.sir.ethz.ch/, 2013.

[5] T. Vögele, M. Eich, F. Grimminger, and K. Fondahl, "A hybrid legged wheel climbing robot for marine inspection," in *Proceedings of International Conference on Climbing and Walking Robots and the Support Tehnologies for Mobile Machines*, 2010.

[6] A. Mazumdar and H. Asada, "Mag-foot: A steel bridge inspection robot," in *Proceedings of International Conference on Intelligent Robots and Systems (IROS)*, 2009.

[7] J. Fang and H. Wang, "Research on the motion system of the inspection robot for 500kv power transmission lines," in *Proceedings of International Conference on Applied Robotics for the Power Industry (CARPI)*, 2010.

[8] L. Christensen, N. Fischer, S. Kroffke, J. Lemburg, and R. Ahlers, "Cost-effective autonomous robots for ballast water tank inspection," *Journal of Ship Production and Design*, vol. 27, pp. 127–136, 8 2011.

[9] D. J. Borgerink, J. Stegenga, D. M. Brouwer, H. J. Woertche, and S. Stramigioli, "Rail-guided robotic end-effector position error due to rail compliance and ship motion," in *IEEE/RSJ International Conference on Intelligent Robots and Systems, IROS 2014, Chicago, IL, USA*, (USA), pp. 3463–3468, IEEE Robotics and Automation Society, September 2014.

[10] B. Siciliano and O. Khatib, eds., *Springer Handbook of Robotics*. Springer, 2008.

[11] S. Stramigioli and H. Bruyninckx, "Geometry and screw theory for robotics," in *Proceedings*, IEEE ICRA, 2001.

[12] S. R. Buss, "Introduction to inverse kinematics with jacobian transpose, pseudoinverse and damped least squares methods," tech. rep., IEEE Journal of Robotics and Automation, 2004.

[13] S. Stramigioli, *From differentiable manifold to interactive robot control*. Whitney, 1998.

[14] B. Siciliano and O. Khatib, *Springer Handbook of Robotics*. Springer, 2008.

8

A   Simulation

This section illustrates the process of two simulations, one successful and one unsuccessful. It is important to notice that most of the time a successful convergence required only a fraction of the timesteps with respect to an unsuccessful simulation. The simulation time for every kinematic structures described in the paper, using 169 relative configurations, ranges from 14m18s for model 2 with 57 failures to 2m44s for model 3 with no failures. There was no optimization done to run the code faster by e.g. parallel threads. Simulation was done on a Intel® Core™i7-2630 CPU @2.00 Ghz, using 12Gb of RAM, and MATLAB 2013a.

A.1   Successful convergence

In figure A.1 some results of a simulation can be seen. In this case the kinematic model is able to postition its end-effector in the desired pose. Due to the choice of the constant stiffness matrix K, the position error dominates the behavior during the first timesteps. At $t = 114$, the end-effector is within the position and orientation criterion and the simulation ends. The intermediate configurations of the kinematic model are shown in overlay in figure A.2.
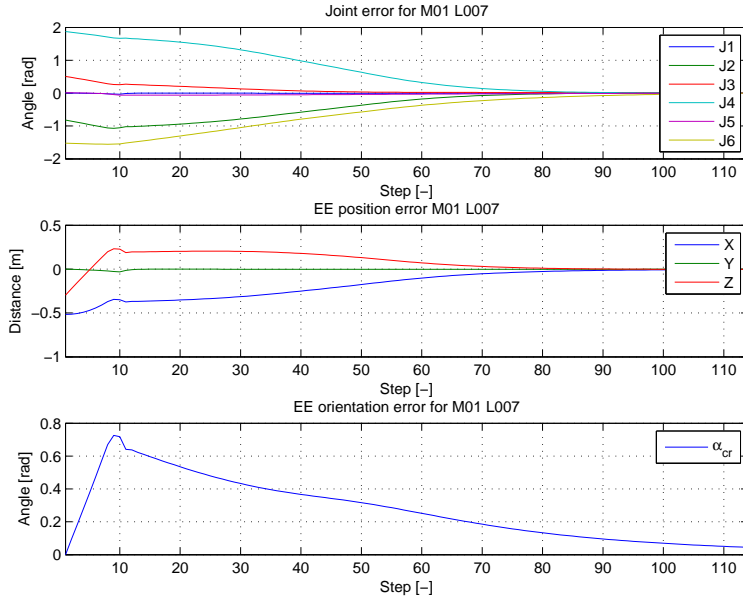
Figure A.1: Trajectory of joint error, end-effector position error and end-effector orientation error, for manipulator 1, location 7.

The joint error represents the amount of rotation the joint has to make to end in the last time step of the simulation.
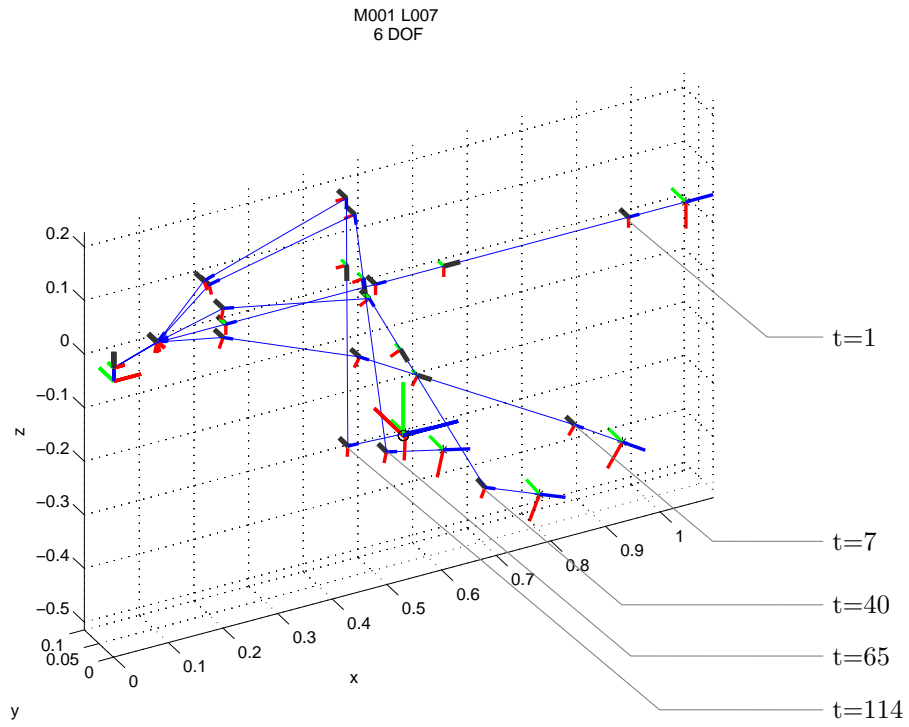
Figure A.2: Overlay in isometric view of kinematic model of manipulator 1, location 7, during simulation at timestep t=1, 7, 40, 65 and 114.

A.2 Unsuccessful convergence

In figure A.3 the results of a simulation with an unsuccessful convergence is shown. As can be seen from figure A.4b the end-effector has not reached the desired pose, therefore the wrench is non-zero. But the current configuration and the choice of the stiffness matrix K yield a static equilibrium. Therefore, therefore no joint motion is induced, and the mechanism stays in the current configuration for the rest of the simulation.
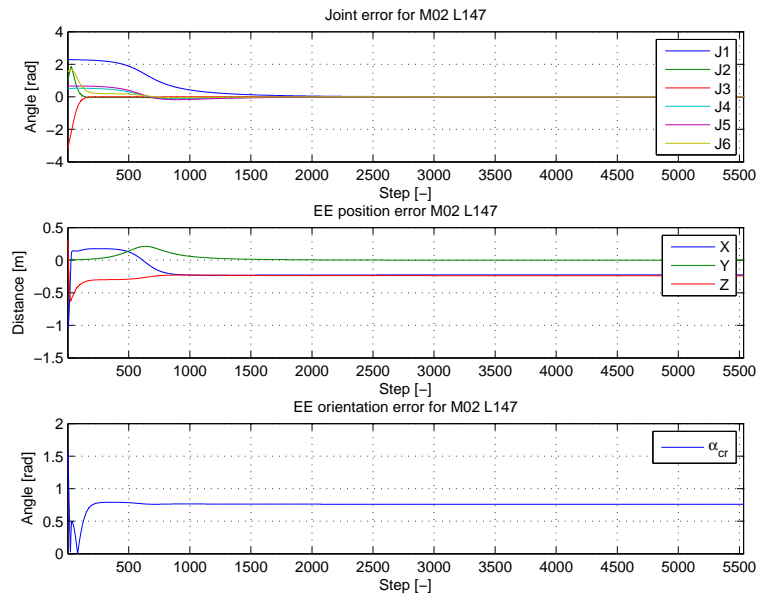
Figure A.3: Trajectory of joint error, end-effector position error and end-effector orientation error, for manipulator 2, location 147.
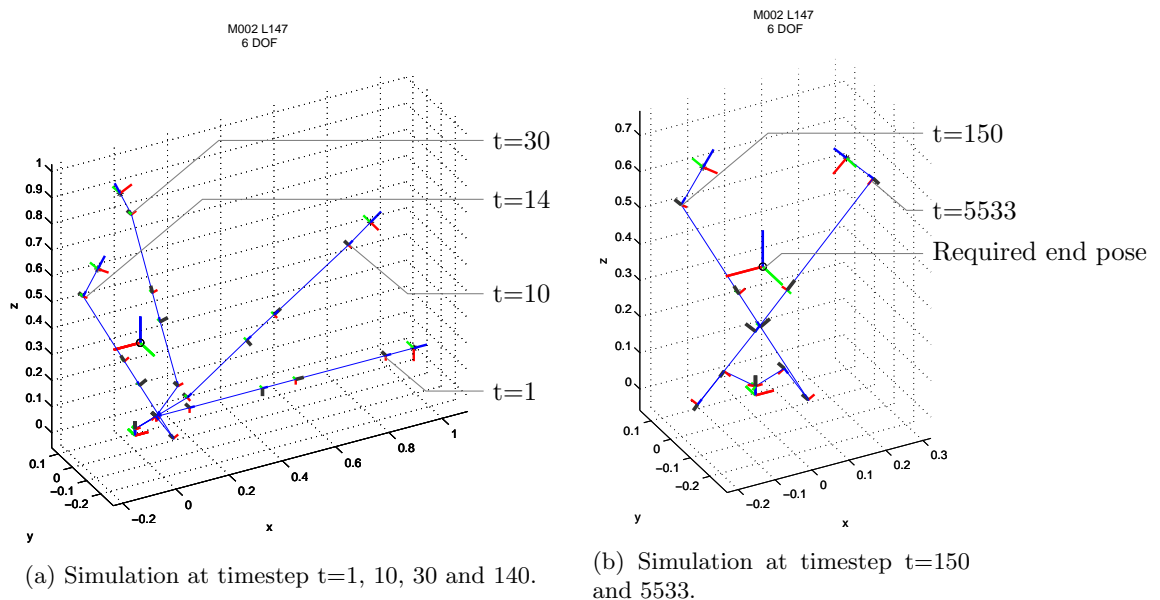
(a) Simulation at timestep t=1, 10, 30 and 140.

(b) Simulation at timestep t=150 and 5533.

Figure A.5: Overlay in isometric view of kinematic model of manipulator 2, location 147, during simulation at different timesteps.

B   Elastic wrench

This section is taken from [1, par 6.4.3]. It describes the algorithm to obtain an elastic wrench between two bodies. It is included as a quick reference for the reader. Figure B.1 illustrates the concept.

1. Choose a relative position r_i^j of minimal potential energy.

2. In this relative position, choose a common point which will be the center of stiffness.

3. Choose two coordinate systems Ψ_i and Ψ_j for i and j respectively, which have their origin in the center of stiffness and coincide at the equilibrium relative position r_i^j.

4. Choose the desired K_t, K_o, K_c which are expressed at equilibrium in the frames $\Psi_i = \Psi_j$.

5. Calculate the corresponding G_t, G_o, G_c with

$$G_x = \frac{1}{2}\mathrm{tr}(K_x)I - K_x \tag{1}$$

6. With H_i^j, the total wrench generated by the spring on body i and expressed in Ψ_i is the sum of the wrenches of the orientational, translational and coupling energies $\bar{W}^i = \begin{bmatrix} (m^i)^T & (f^i)^T \end{bmatrix}$ with:

$$\tilde{m}^i = -2\mathrm{as}(G_o R_i^j) - \mathrm{as}(G_t R_j^i \tilde{p}_i^j \tilde{p}_i^j R_i^j) - 2\mathrm{as}(G_c \tilde{p}_i^j R_i^j) \tag{2}$$

$$\tilde{f}^i = -R_j^i \mathrm{as}(G_t \tilde{p}_i^j) R_i^j - \mathrm{as}(G_t R_j^i \tilde{p}_i^j R_i^j) - 2\mathrm{as}(G_c R_i^j) \tag{3}$$

$$\tag{4}$$

where

$$\mathrm{as(A)} := \frac{1}{2}(A - A^T) \tag{5}$$

7. The wrench $\bar{W}^j$ that the spring applies to body j will be $\bar{W}^j = -Ad_{H_j^i}^T \bar{W}^i$, which implies that:

$$m^j = -R_j^i m^i - \tilde{p}_i^j R_i^j f^i \tag{6}$$

$$f^j = -R_i^j f^i \tag{7}$$
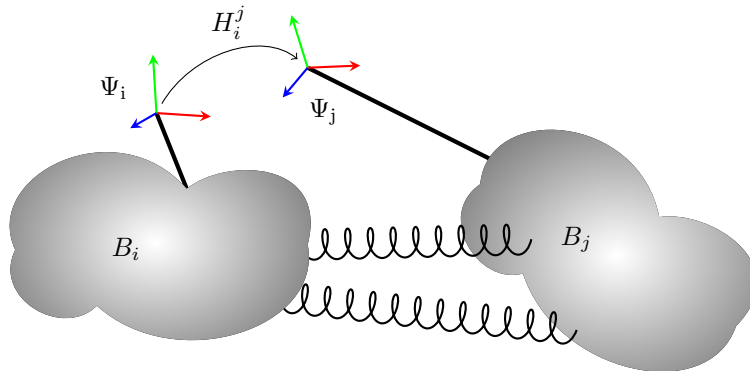
Figure B.1: Spatial spring connecting two bodies.

C Proof-of-principle

C.1 Dynamixel

Dynamixels are a package consisting of a Maxon motor, a 225 : 1 spur gear reduction, a ball bearing supported output shaft fitted with a hall-effect absolute position sensor and an ARM Cortex-M3 microcontroller from STMicroelectronics. The Maxon motor is custom, but based on type 222036, and has the following specs:

Nominal voltage	9 V
Nominal torque	10.8 mN m
Maximum torque	52.4 mN m

The ideal maximum torque at the output shaft is $52.4\,\text{mN m} \cdot 225 = 11.7\,\text{N m}$. This matches quite well with the listed stall torque listed by the supplier, 10.0 N m. Unfortunately during testing in the lab, the motors failed to match these specs. One of the major disadvantages is the proprietary firmware disabling the Dynamixel at approximately 5 N m.

C.2 Bearing

The bearing on the output shaft of the Dynamixels insufficient for support of the roll-joints. Especially for the first joint which needs to support a bending moment of approximately: $1\,\text{m} \cdot 1\,\text{kg} = 9.81\,\text{N m}$ A solution was found in the form of a crossed roller bearing type shown in figure C.1. The bearing consist of a low height, large inner and large outer diameter. The circular raceway is occupied by rollers of witch the orientation alternates.
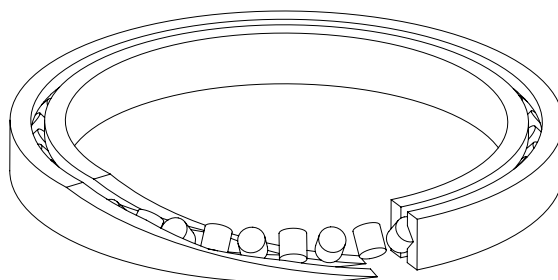
Figure C.1: A crossed roller bearing, with a partial cut-out of the inner and outer raceway. Type: THK RA7008C-UU-C, with ID=70 mm, OD=86 mm, W=8 mm, Basic radial load rating=5.98 kN

According to the datasheet [2], the equivalent radial load for a given moment can be calculated according to:

$$P_0 = X_0 \cdot \left(F_r + \frac{2M}{dp} \right) + Y_0 \cdot F_a \qquad (8)$$

where the parameters for a load of 10 N applied at a arm length of 1 m are

X_0	Static radial factor	$X_0 = 1$
F_r	Radial load	10 N
Y_0	Static axial factor	$Y_0 = 0.44$
M	Moment	10 N m
F_a	Axial load	0 N
dp	Roller pitch circle diameter	0.77 m

the static equivalent radial load, P_0, becomes 269 N m, which is well below the specs of 5.98 kN.

C.3   Joint 1 gear

For joint 1 the output torque of the Dynamixel is insufficient to connect directly. A timing belt of type GT2 in combination with some gears proofed to be a good solution. The primary gear, attached to the Dynamixel mounted on link 1, has 36 teeth, and the secondary gear, attached to the link 0, has 110 teeth. The 110 teeth gear is a size which can not be ordered, therefore it was custom made at the university using a stack of laser cutted steel plates. This is a cheap and relative fast way to obtain the part. The assembly is shown in figure C.2.
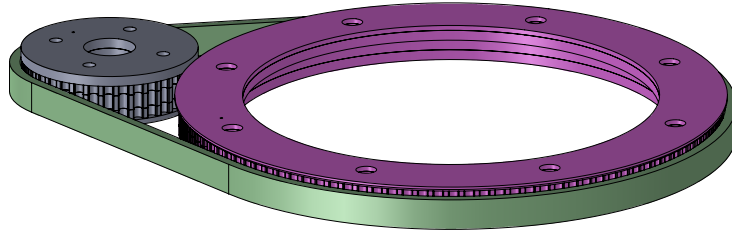
Figure C.2: Gear assembly with 110:36 ratio. The gears are built from a stack of 2, 3 and 2mm steel plate.

C.4   Asymmetric link

In the paper is stated that an asymmetric link can introduce a local minimum. Although this is a disadvantage of the asymmetry, it offers a major advantage in terms of workspace reachability. In figure C.3 it can be seen that joint 2 has an offset of 80 mm. Hereby link 2 can position joint 4 to the opposite side of the rail on which the carrier is mounted, without collision with the rail.
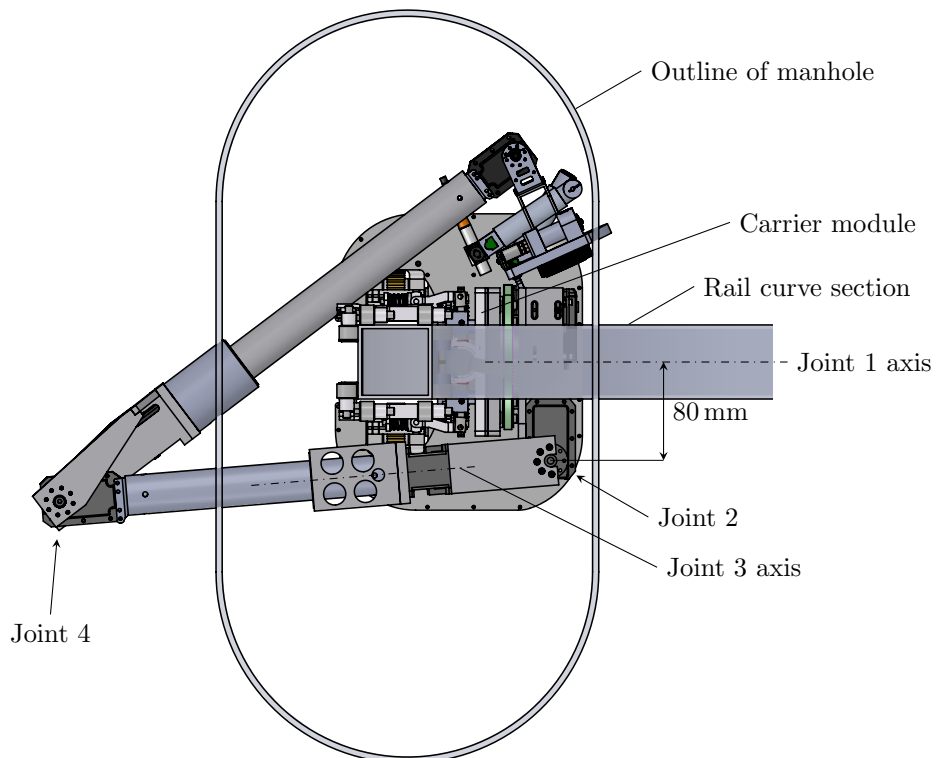
Figure C.3: Asymmetric link 1 makes joint 2 offset by 80 mm which allows link 2 to put joint 4 to the opposite side of the rail with respect to the base.

C.5   Sleeve bearing

For joint 3 and 5 the output shaft of the Dynamixels is unable to withstand the bending torque. A solution was found in a design where the Dynamixel is mounted to an aluminium housing, and a nylon bushing is placed coaxial at a distance of 60 mm of the housing. In figure C.4 a drawing of joint 4 can be seen.
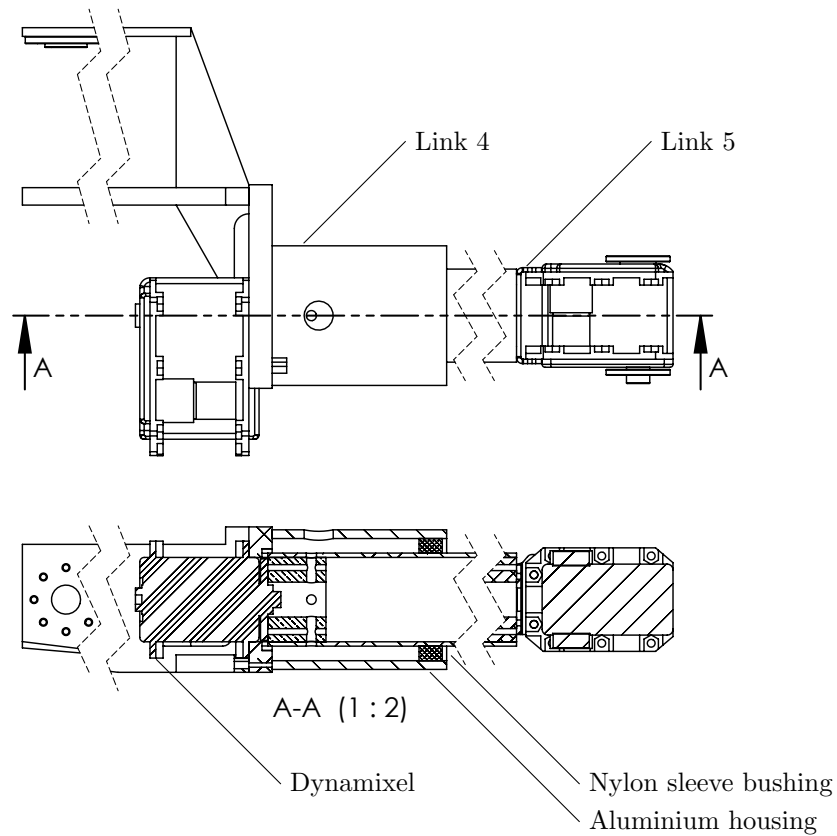
Figure C.4: Drawing of roll-joint 5 assembly connecting link 4 and link 5. Section view A-A shows the nylon sleeve bushing.

References

[1] S. Stramigioli, *From differentiable manifold to interactive robot control.* Whitney, 1998.

[2] THK, "Cross-roller ring series, catalog no.382-3e." `https://tech.thk.com/upload/catalog_claim/pdf/382E_CrossRollerRing.pdf`, march 2015. original document from THK website.